Introduction to Nuclear and Particle Physics

β decay

Helga Dénes 2022 Yachay Tech

hdenes@yachaytech.edu.ec

Mass parabola - discussed related to the binding energy

β decay

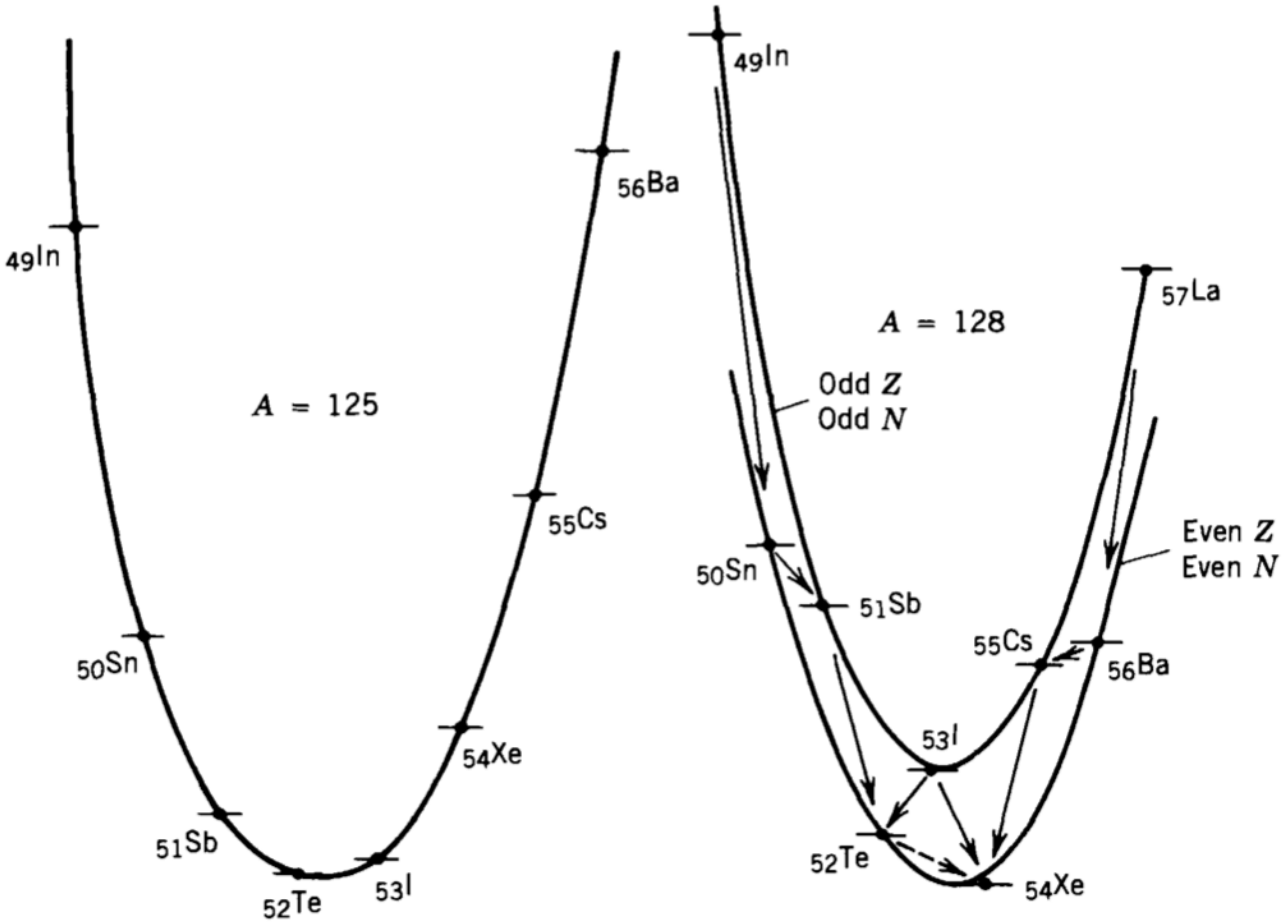

Figure 3.18 Mass chains for $A = 125$ and $A = 128$. For $A = 125$, note how the energy differences between neighboring isotopes increase as we go further from the stable member at the energy minimum. For $A = 128$, note the effect of the pairing term; in particular, ^{128}I can decay in either direction, and it is energetically possible for ^{128}Te to decay directly to ^{128}Xe by the process known as double β decay.

β decay - continuous energy distribution

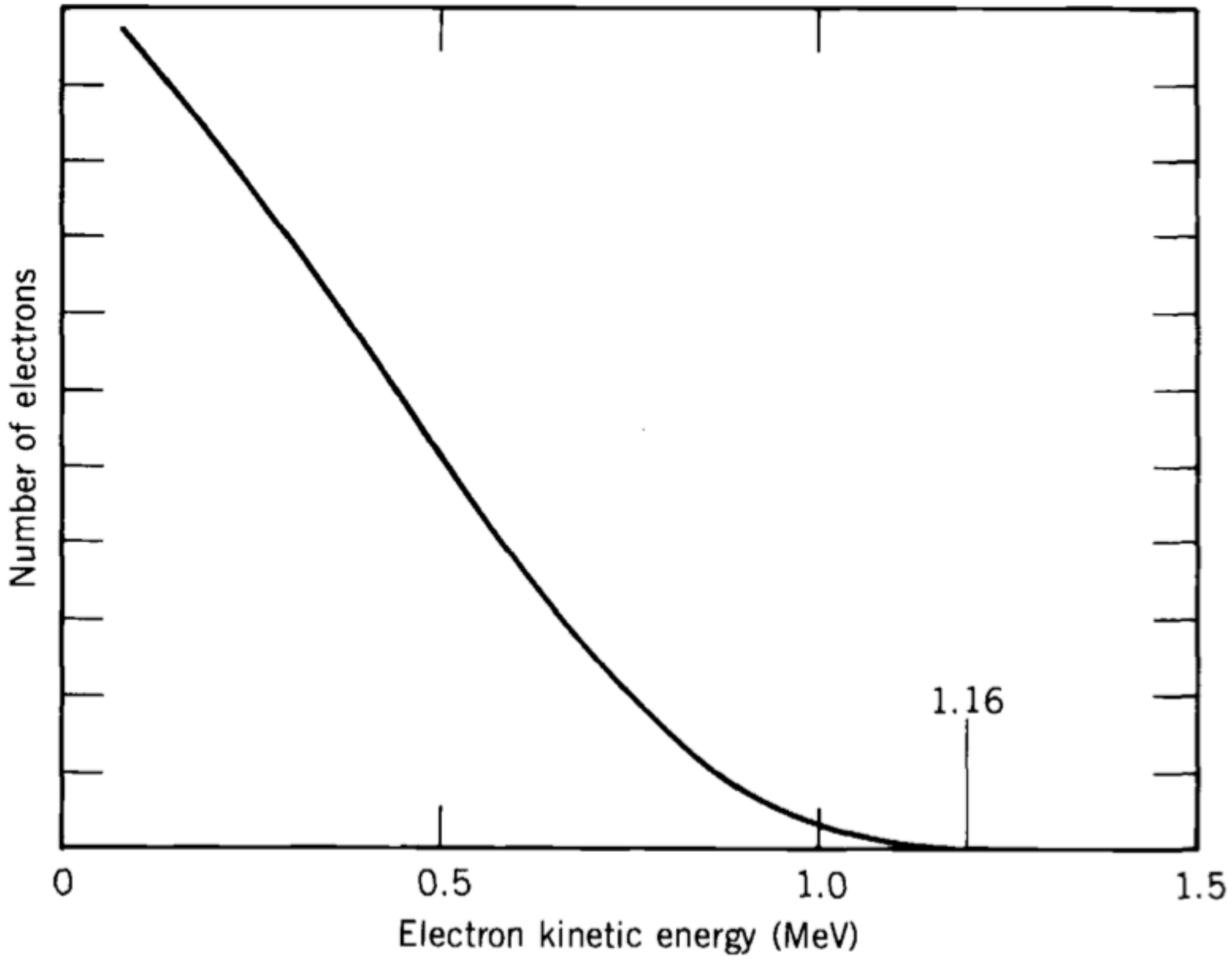

Figure 9.1 The continuous electron distribution from the β decay of ^{210}Bi (also called RaE in the literature).

β decay - continuous energy distribution

Table 9.1 Typical β-Decay Processes

Decay	Type	Q (MeV)	$t_{1/2}$
$^{23}Ne \to {}^{23}Na + e^- + \bar{\nu}$	β^-	4.38	38 s
$^{99}Tc \to {}^{99}Ru + e^- + \bar{\nu}$	β^-	0.29	2.1×10^5 y
$^{25}Al \to {}^{25}Mg + e^+ + \nu$	β^+	3.26	7.2 s
$^{124}I \to {}^{124}Te + e^+ + \nu$	β^+	2.14	4.2 d
$^{15}O + e^- \to {}^{15}N + \nu$	ε	2.75	1.22 s
$^{41}Ca + e^- \to {}^{41}K + \nu$	ε	0.43	1.0×10^5 y

β decay - continuous energy distribution

Predicted

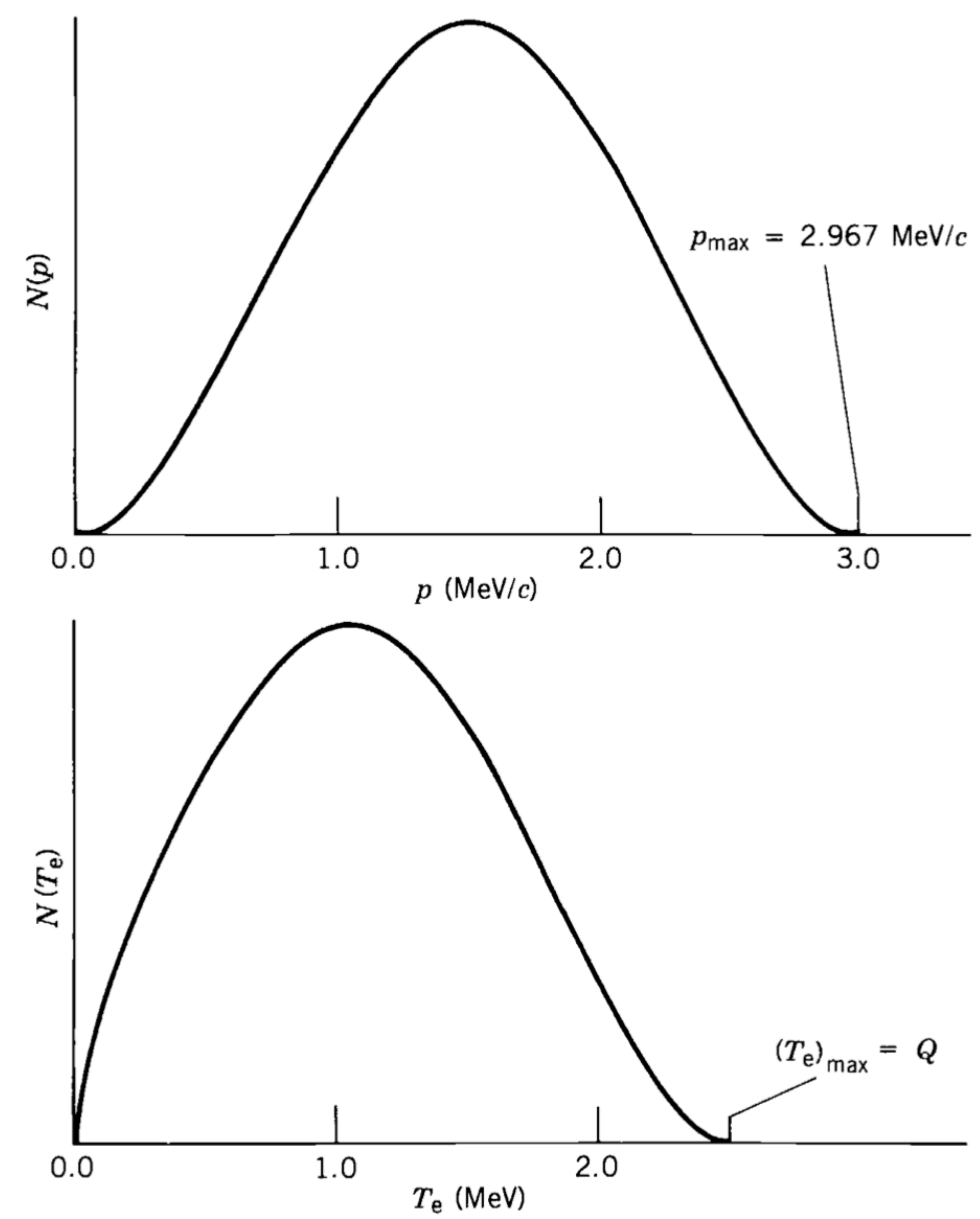

Figure 9.2 Expected electron energy and momentum distributions, from Equations 9.24 and 9.25. These distributions are drawn for $Q = 2.5$ MeV.

Detected

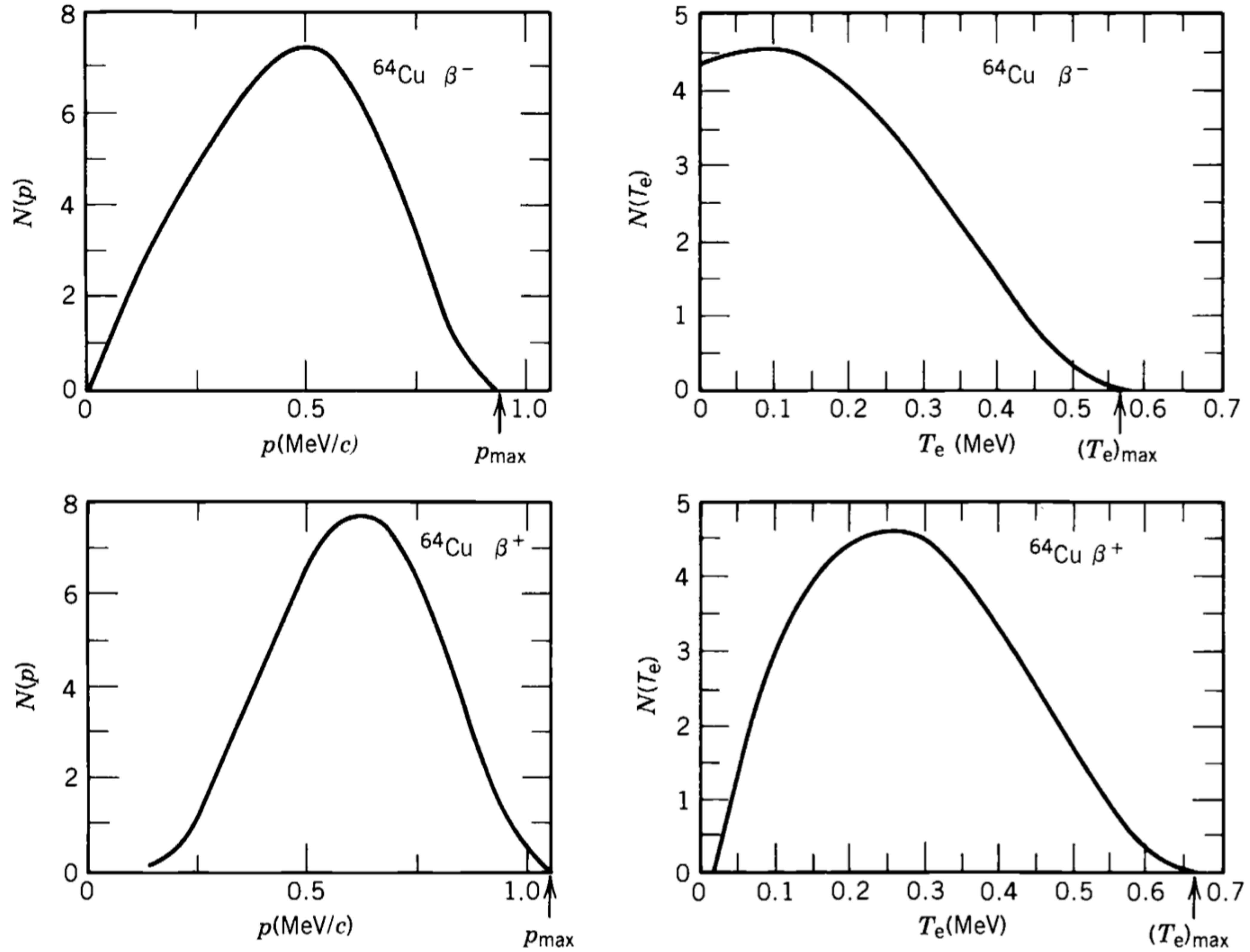

Figure 9.3 Momentum and kinetic energy spectra of electrons and positrons emitted in the decay of ^{64}Cu. Compare with Figure 9.2; the differences arise from the Coulomb interactions with the daughter nucleus. From R. D. Evans, *The Atomic Nucleus* (New York: McGraw-Hill, 1955).

β decay - Fermi - Kurie plot

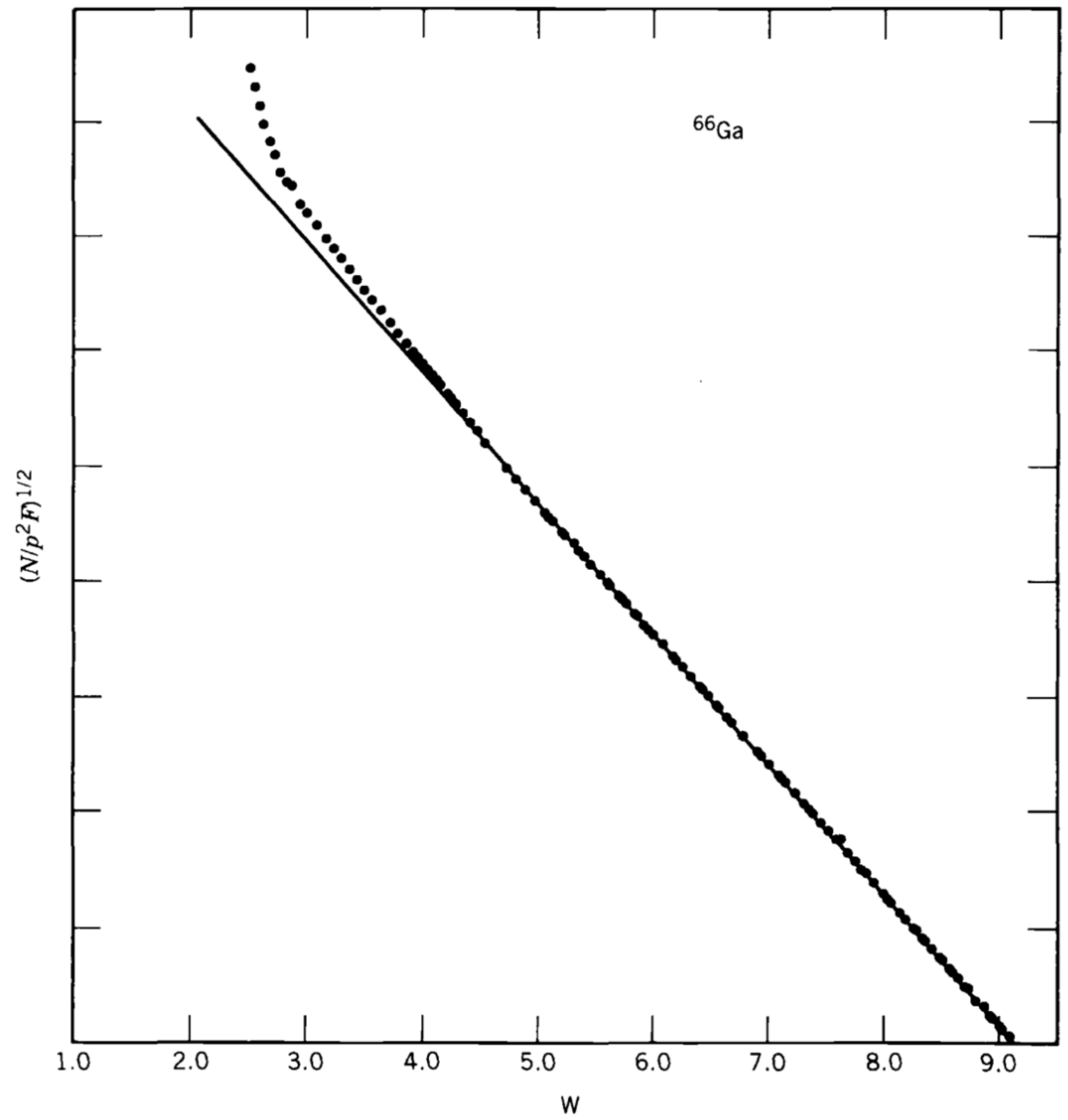

Figure 9.4 Fermi – Kurie plot of allowed $0^+ \rightarrow 0^+$ decay of ^{66}Ga. The horizontal scale is the relativistic *total* energy ($T_e + m_e c^2$) in units of $m_e c^2$. The deviation from the straight line at low energy arises from the scattering of low-energy electrons within the radioactive source. From D. C. Camp and L. M. Langer, *Phys. Rev.* **129**, 1782 (1963).

β decay - Fermi - Kurie plot

Uncorrected

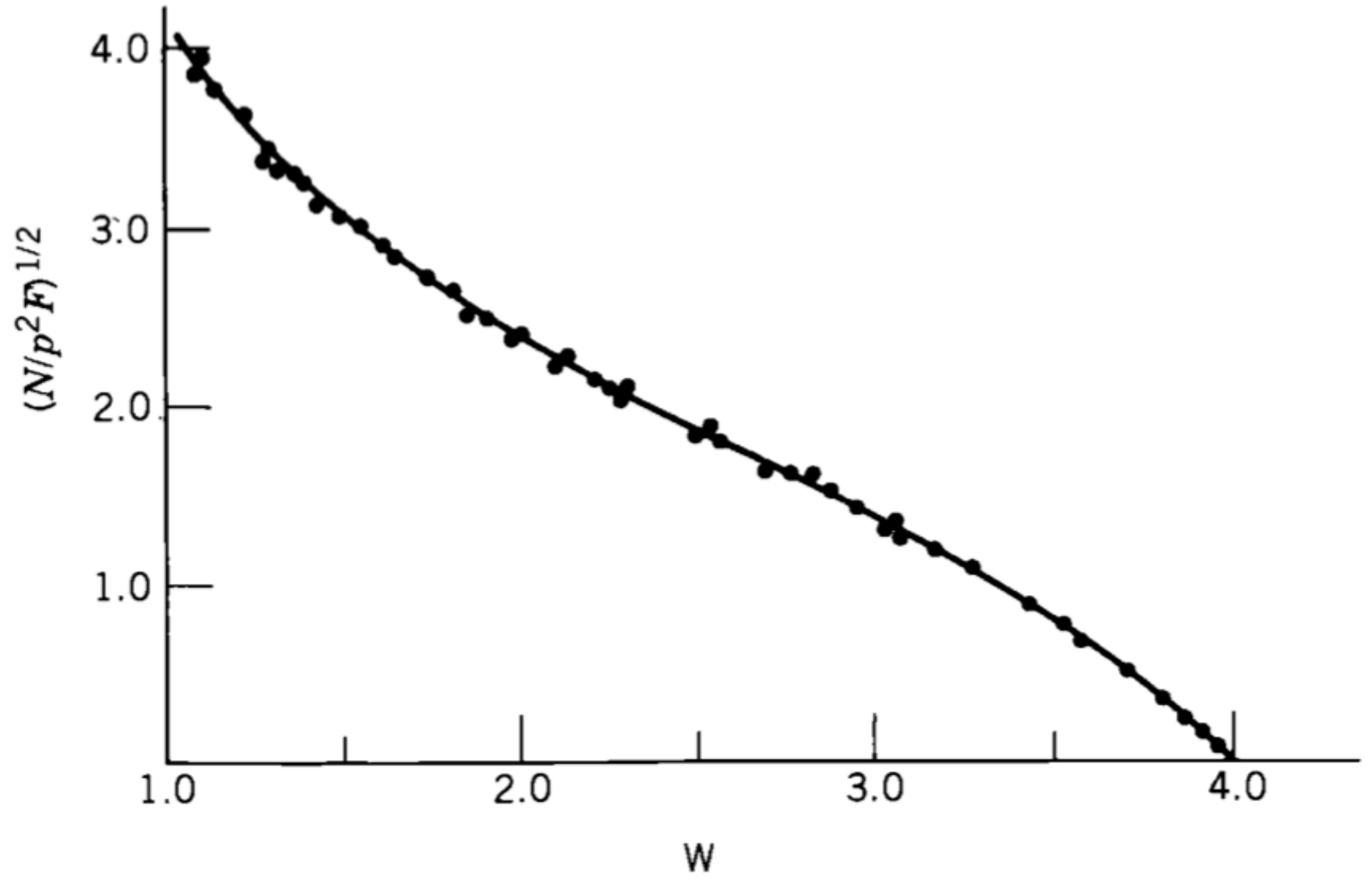

corrected

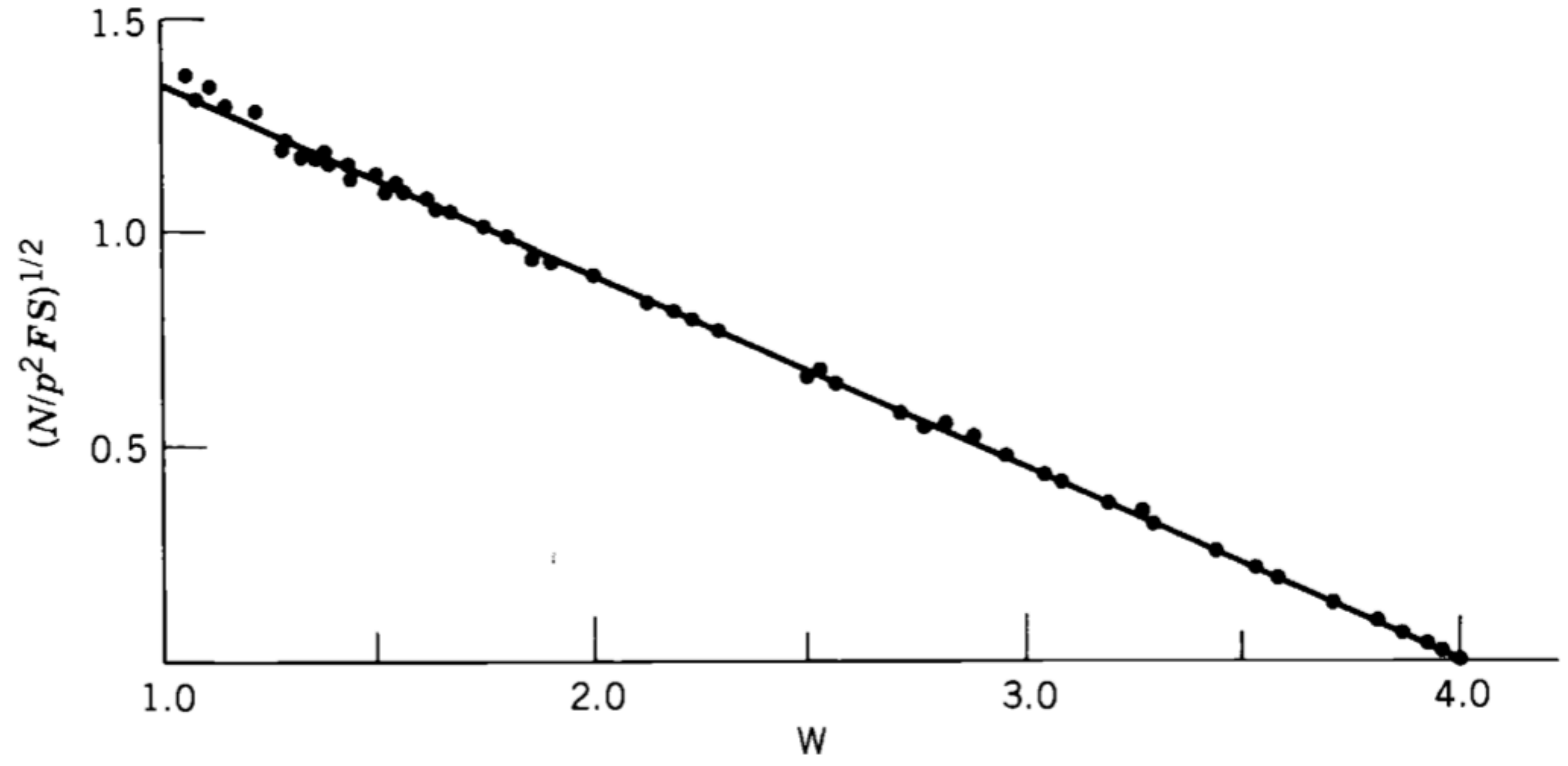

Figure 9.5 Uncorrected Fermi – Kurie plot in the β decay of ^{91}Y (top). The linearity is restored if the shape factor $S(p, q)$ is included; for this type of first-forbidden decay, the shape factor $p^2 + q^2$ gives a linear plot (bottom). Data from L. M. Langer and H. C. Price, *Phys. Rev.* **75**, 1109 (1949).

β decay

Table 9.2 *ft* Values for $0^+ \rightarrow 0^+$ Superallowed Decays

Decay	*ft* (s)
$^{10}C \rightarrow {}^{10}B$	3100 ± 31
$^{14}O \rightarrow {}^{14}N$	3092 ± 4
$^{18}Ne \rightarrow {}^{18}F$	3084 ± 76
$^{22}Mg \rightarrow {}^{22}Na$	3014 ± 78
$^{26}Al \rightarrow {}^{26}Mg$	3081 ± 4
$^{26}Si \rightarrow {}^{26}Al$	3052 ± 51
$^{30}S \rightarrow {}^{30}P$	3120 ± 82
$^{34}Cl \rightarrow {}^{34}S$	3087 ± 9
$^{34}Ar \rightarrow {}^{34}Cl$	3101 ± 20
$^{38}K \rightarrow {}^{38}Ar$	3102 ± 8
$^{38}Ca \rightarrow {}^{38}K$	3145 ± 138
$^{42}Sc \rightarrow {}^{42}Ca$	3091 ± 7
$^{42}Ti \rightarrow {}^{42}Sc$	3275 ± 1039
$^{46}V \rightarrow {}^{46}Ti$	3082 ± 13
$^{46}Cr \rightarrow {}^{46}V$	2834 ± 657
$^{50}Mn \rightarrow {}^{50}Cr$	3086 ± 8
$^{54}Co \rightarrow {}^{54}Fe$	3091 ± 5
$^{62}Ga \rightarrow {}^{62}Zn$	2549 ± 1280

β decay - neutrino mass

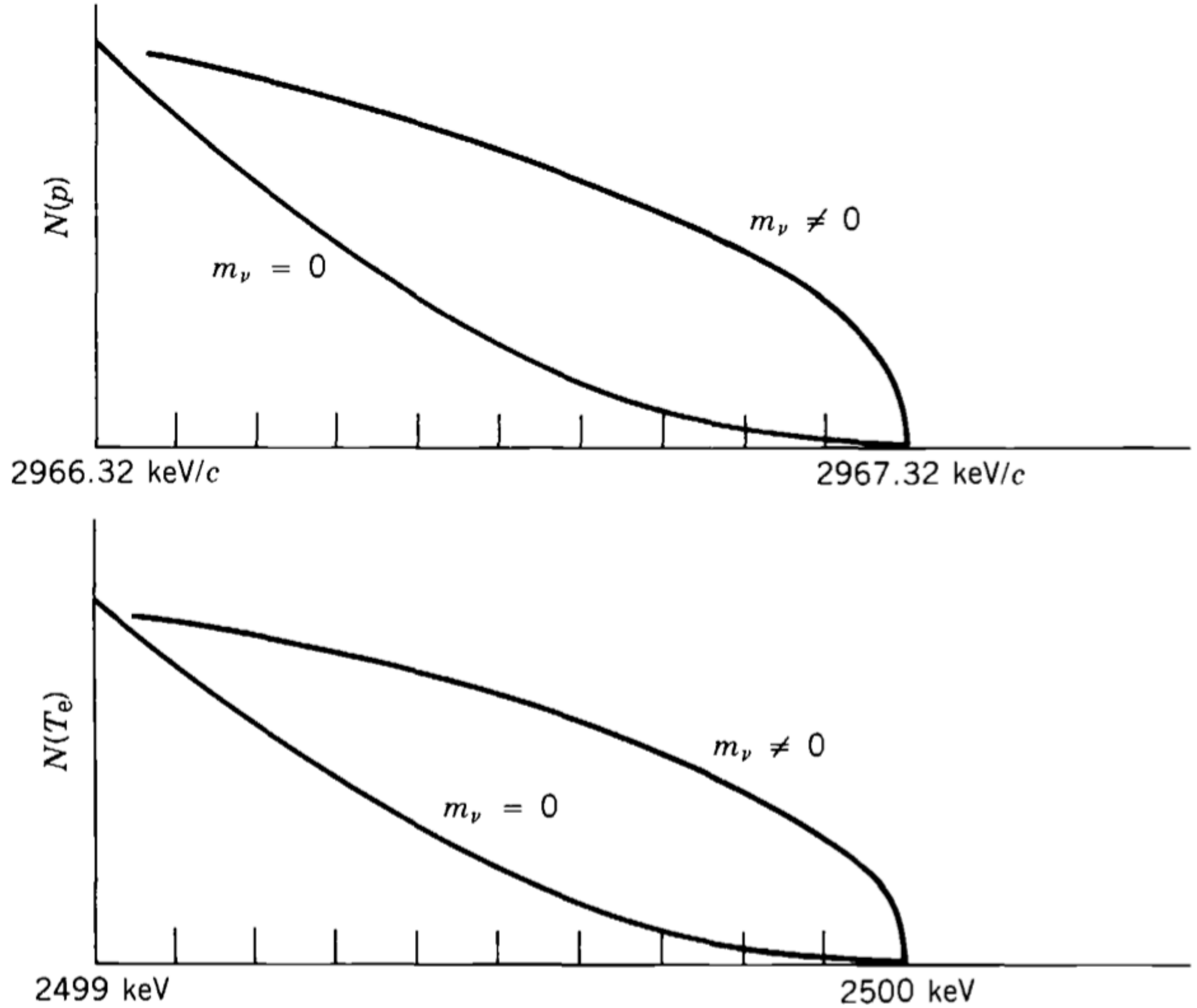

Figure 9.6 Expanded view of the upper 1-keV region of the momentum and energy spectra of Figure 9.2. The normalizations are arbitrary; what is significant is the difference in the shape of the spectra for $m_\nu = 0$ and $m_\nu \neq 0$. For $m_\nu = 0$, the slope goes to zero at the endpoint; for $m_\nu \neq 0$, the slope at the endpoint is infinite.

β decay - neutrino mass

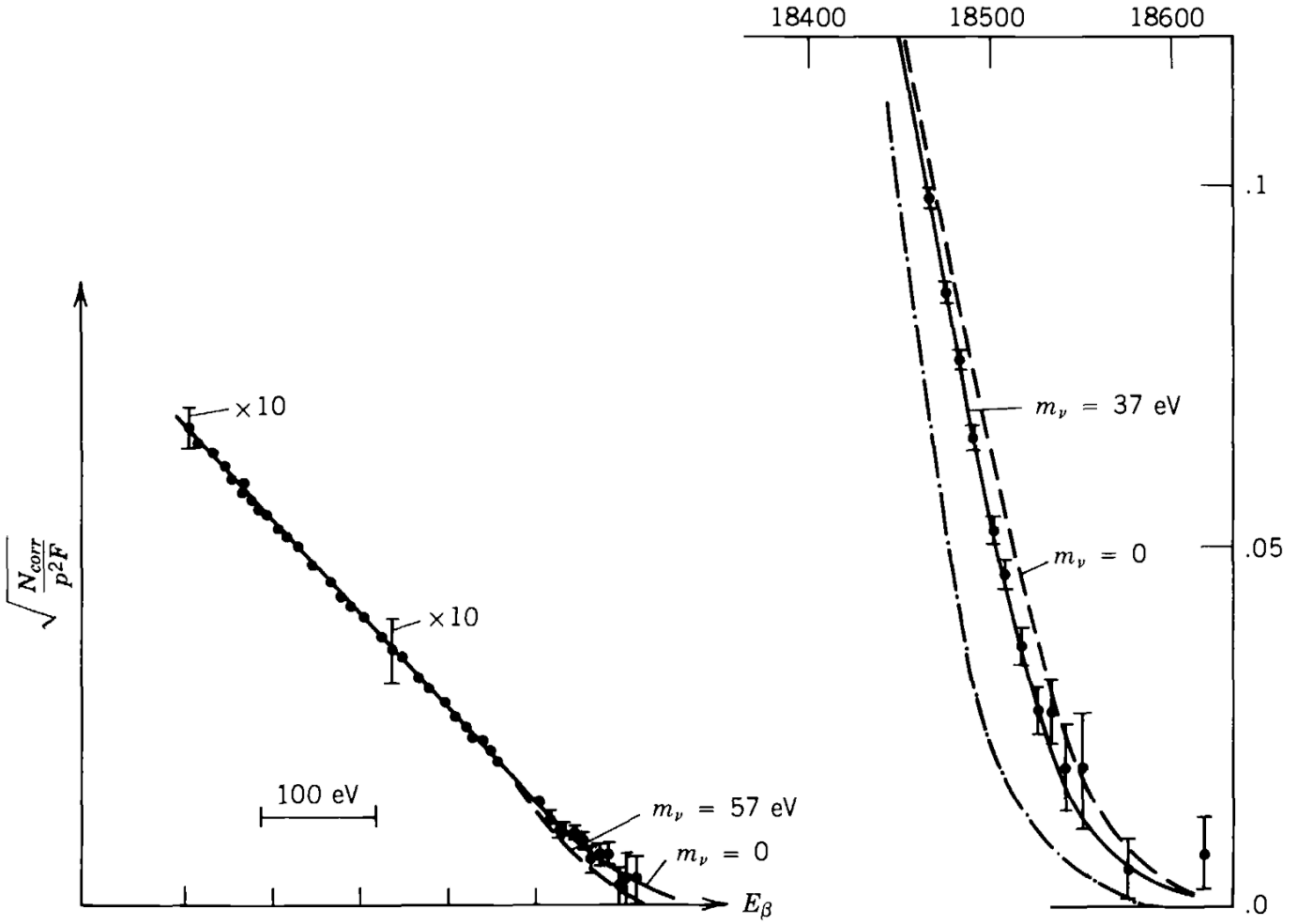

Figure 9.7 Experimental determination of the neutrino mass from the β decay of tritium (^3H). The data at left, from K.-E. Bergkvist, *Nucl. Phys. B* **39**, 317 (1972), are consistent with a mass of zero and indicate an upper limit of around 60 eV. The more recent data of V. A. Lubimov et al., *Phys. Lett. B* **94**, 266 (1980), seem to indicate a nonzero value of about 30 eV; however, these data are subject to corrections for instrumental resolution and atomic-state effects and may be consistent with a vanishing mass.

β decay - ratios

Table 9.3 Ratio of Fermi to Gamow-Teller Matrix Elements

	Decay	$y = g_F M_F / g_{GT} M_{GT}$	%F	%GT
Mirror decays	$n \rightarrow p$	0.467 ± 0.003	18	82
	$^{3}H \rightarrow {}^{3}He$	0.479 ± 0.001	19	81
	$^{13}N \rightarrow {}^{13}C$	1.779 ± 0.006	76	24
	$^{21}Na \rightarrow {}^{21}Ne$	1.416 ± 0.012	67	33
	$^{41}Sc \rightarrow {}^{41}Ca$	0.949 ± 0.003	47	53
Nonmirror decays	$^{24}Na \rightarrow {}^{24}Mg$	-0.021 ± 0.007	0.044	99.956
	$^{41}Ar \rightarrow {}^{41}K$	$+0.027 \pm 0.011$	0.073	99.927
	$^{46}Sc \rightarrow {}^{46}Ti$	-0.023 ± 0.005	0.053	99.947
	$^{52}Mn \rightarrow {}^{52}Cr$	-0.144 ± 0.006	2	98
	$^{65}Ni \rightarrow {}^{65}Cu$	-0.002 ± 0.019	< 0.04	> 99.96

$\beta\beta$ decay

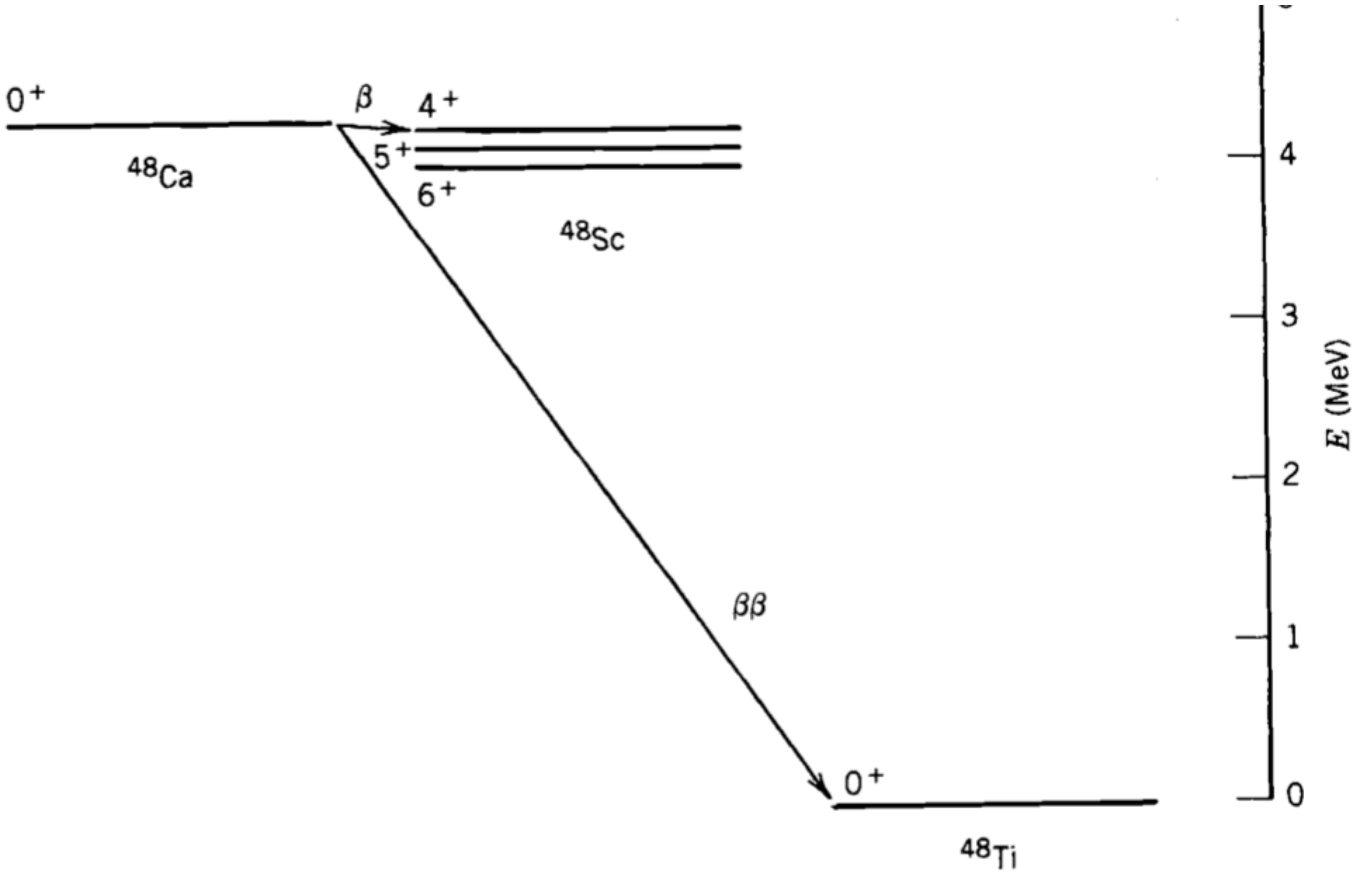

Figure 9.10 The decay of ^{48}Ca. The superallowed $\beta\beta$ decay to ^{48}Ti is an alternative to the fourth-forbidden single-β decay to ^{48}Sc.

$\beta\beta$ decay

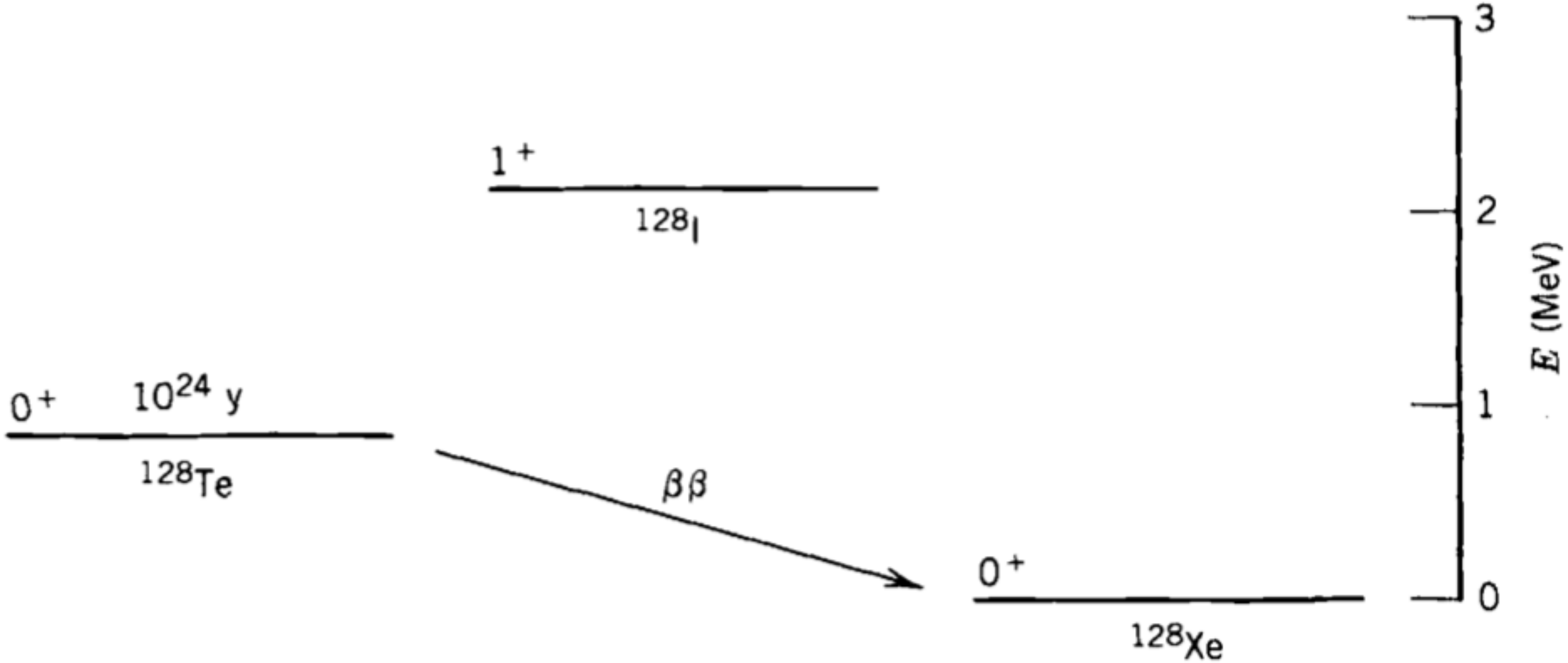

Figure 9.11 Single-β decay of ^{128}Te is energetically forbidden, but $\beta\beta$ decay to ^{128}Xe is possible. See Figure 3.18 to understand the relative masses of these nuclei.

$\beta\beta$ decay

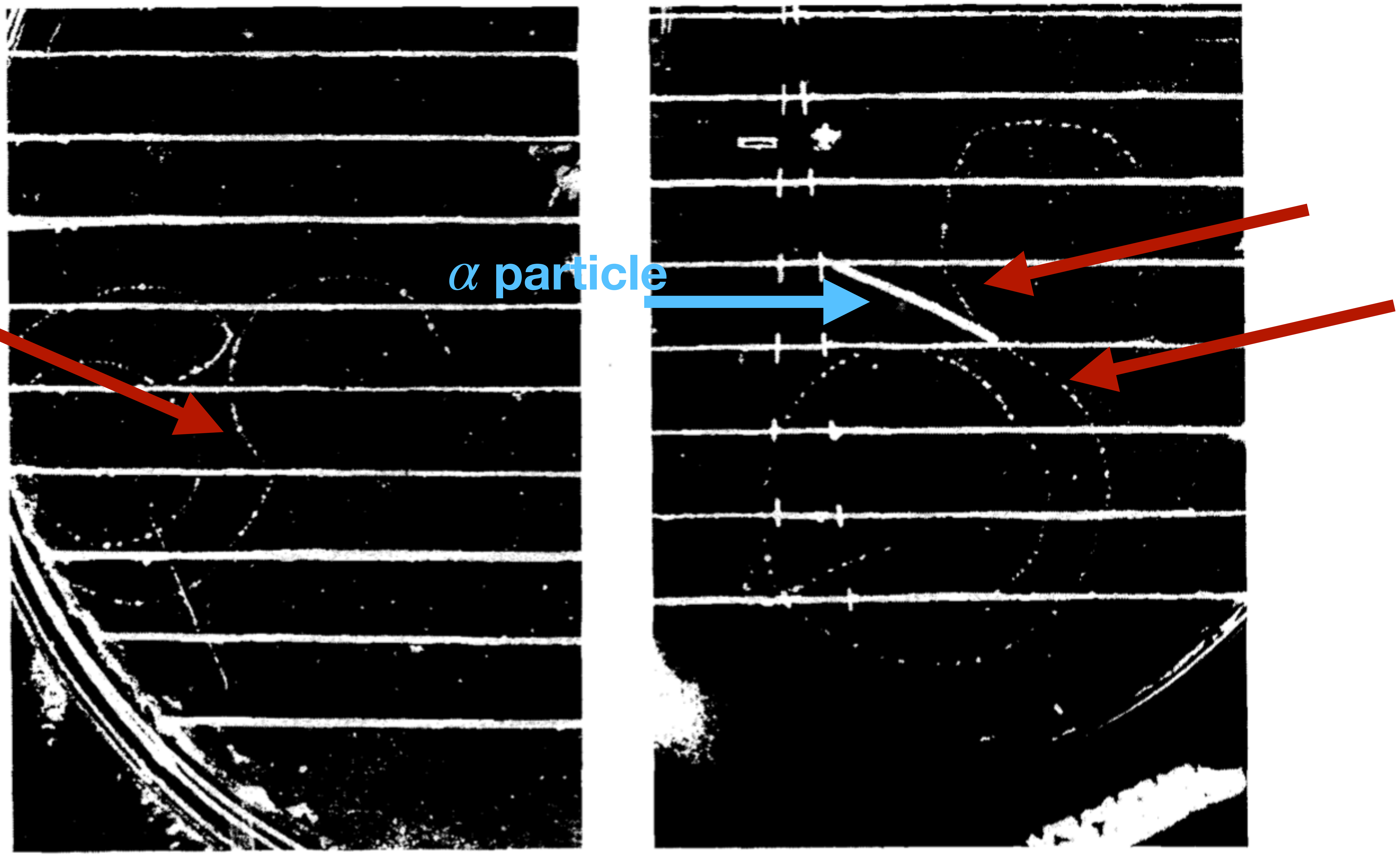

Figure 9.12 Cloud chamber photograph of a suspected $\beta\beta$-decay event from ^{82}Se. The horizontal lines are strips of ^{82}Se source material. The $\beta\beta$-decay event is the pair of curved tracks originating from one of the strips in the exact center of the photograph at left. There are also background events due to natural radioactivity; these produce two β-decay electrons in succession (as in the natural radioactive chain of decays, Figure 6.10) and an α particle. Note the two electron tracks and the heavy α track originating from a common point near the center of the photograph on the right. A magnetic field perpendicular to the plane of the photos curves the tracks, so that the electron momentum can be deduced. From M. K. Moe and D. D. Lowenthal, *Phys. Rev. C* **22**, 2186 (1980).

β-delayed nucleon emission

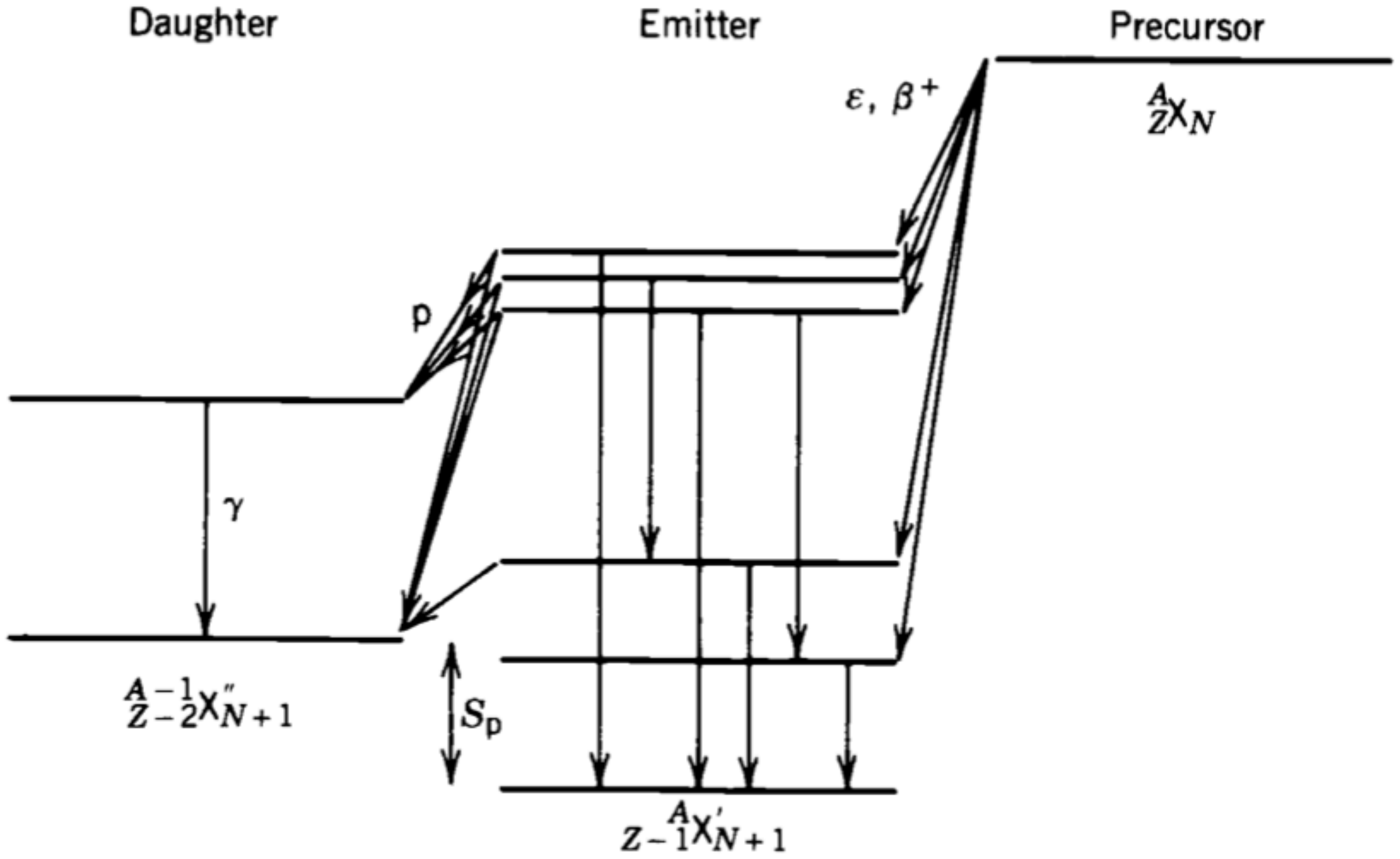

Figure 9.13 Schematic of β-delayed nucleon emission. The β decay of the precursor populates highly excited states in the emitter that are unstable with respect to nucleon emission. Note that the energy of the excited state in the emitter equals the sum of the energy of the emitted nucleon plus the nucleon separation energy between X′ and X″ (plus the small correction for the recoil of the emitting nucleus).

β-delayed nucleon emission

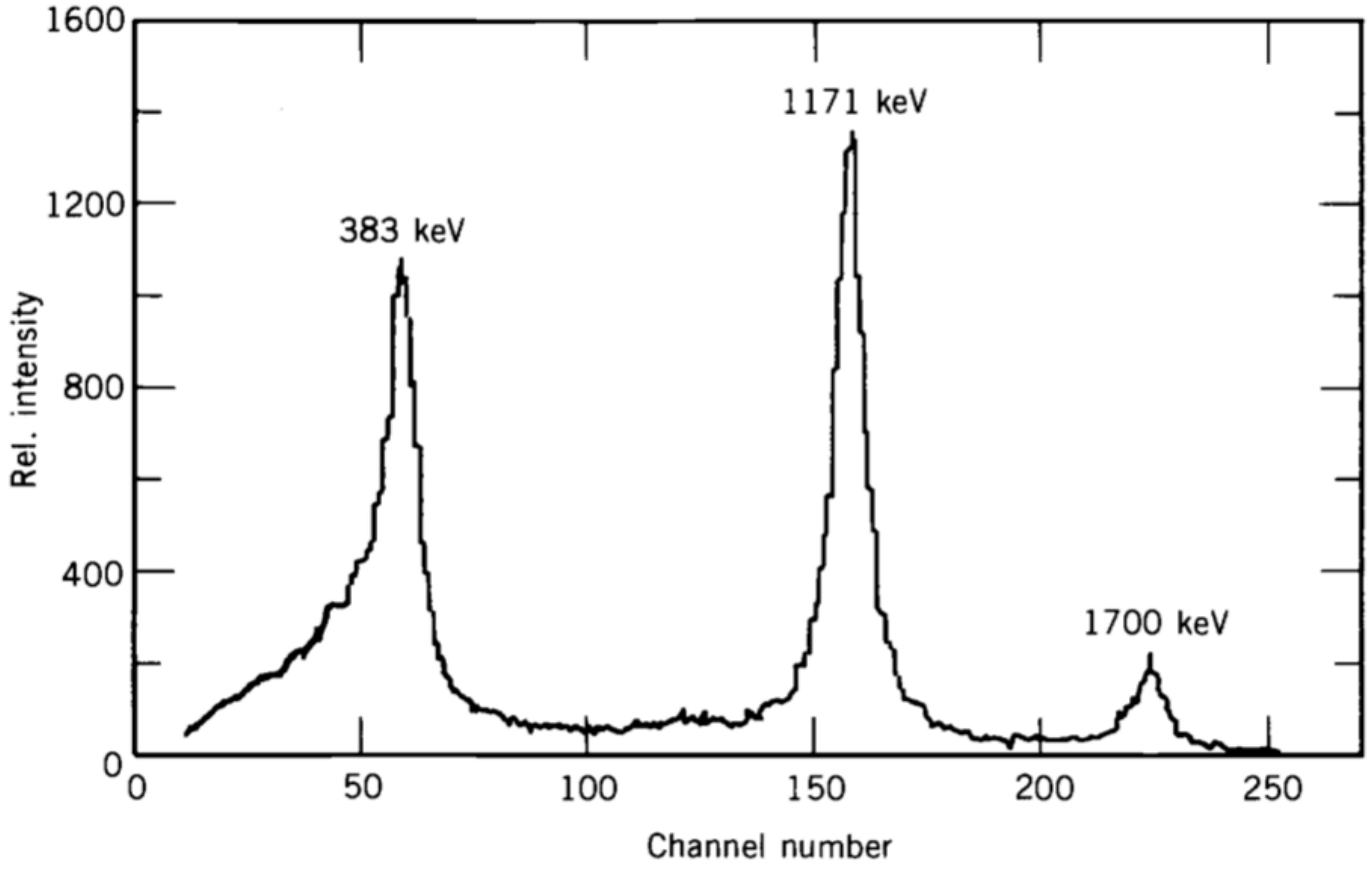

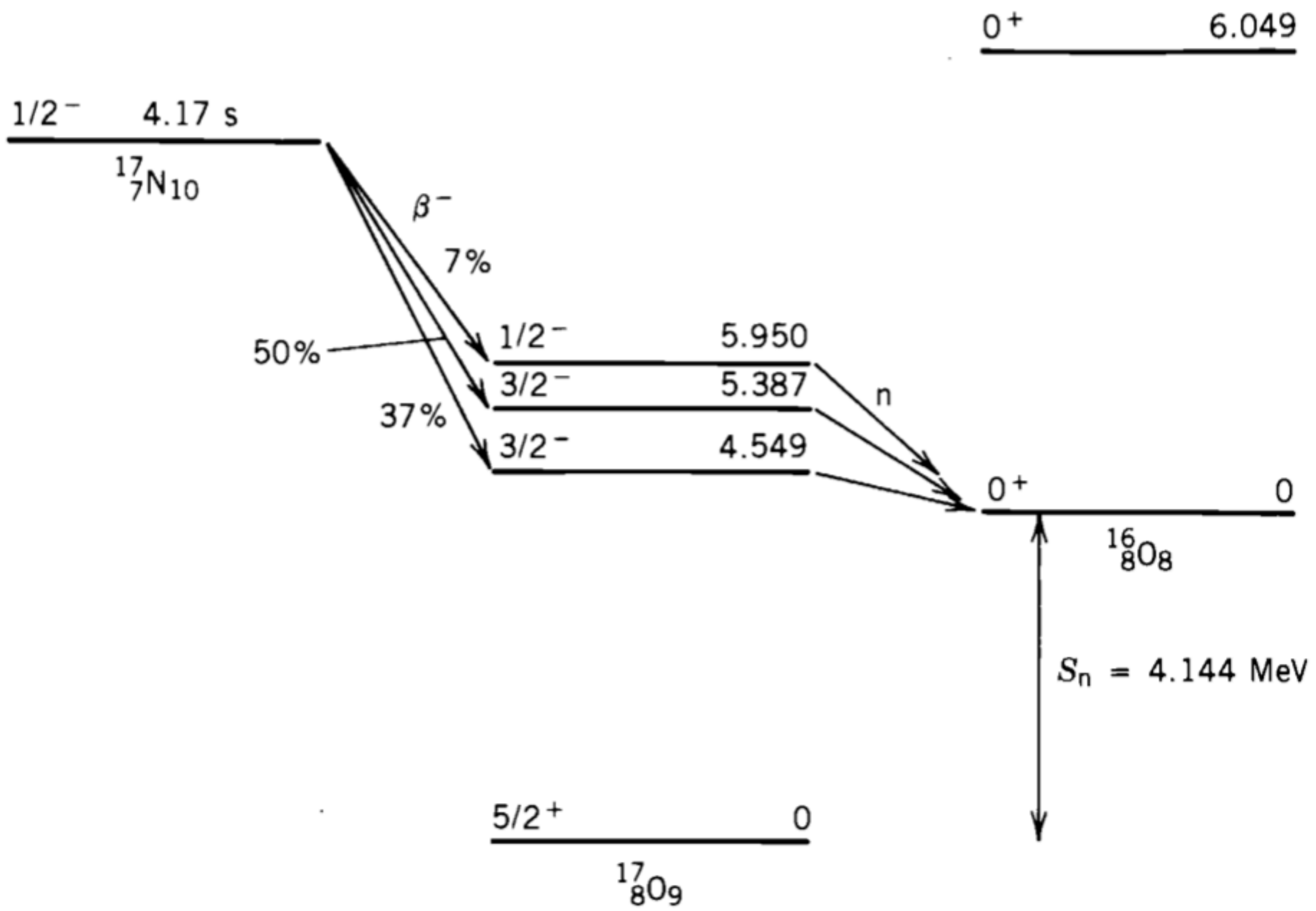

Figure 9.15 The β-delayed neutron decay of ^{17}N.

Figure 9.14 Beta-delayed neutrons following the decay of ^{17}N. The neutron energy spectrum is shown at the left;

Hydrogen Isotopes - XKCD

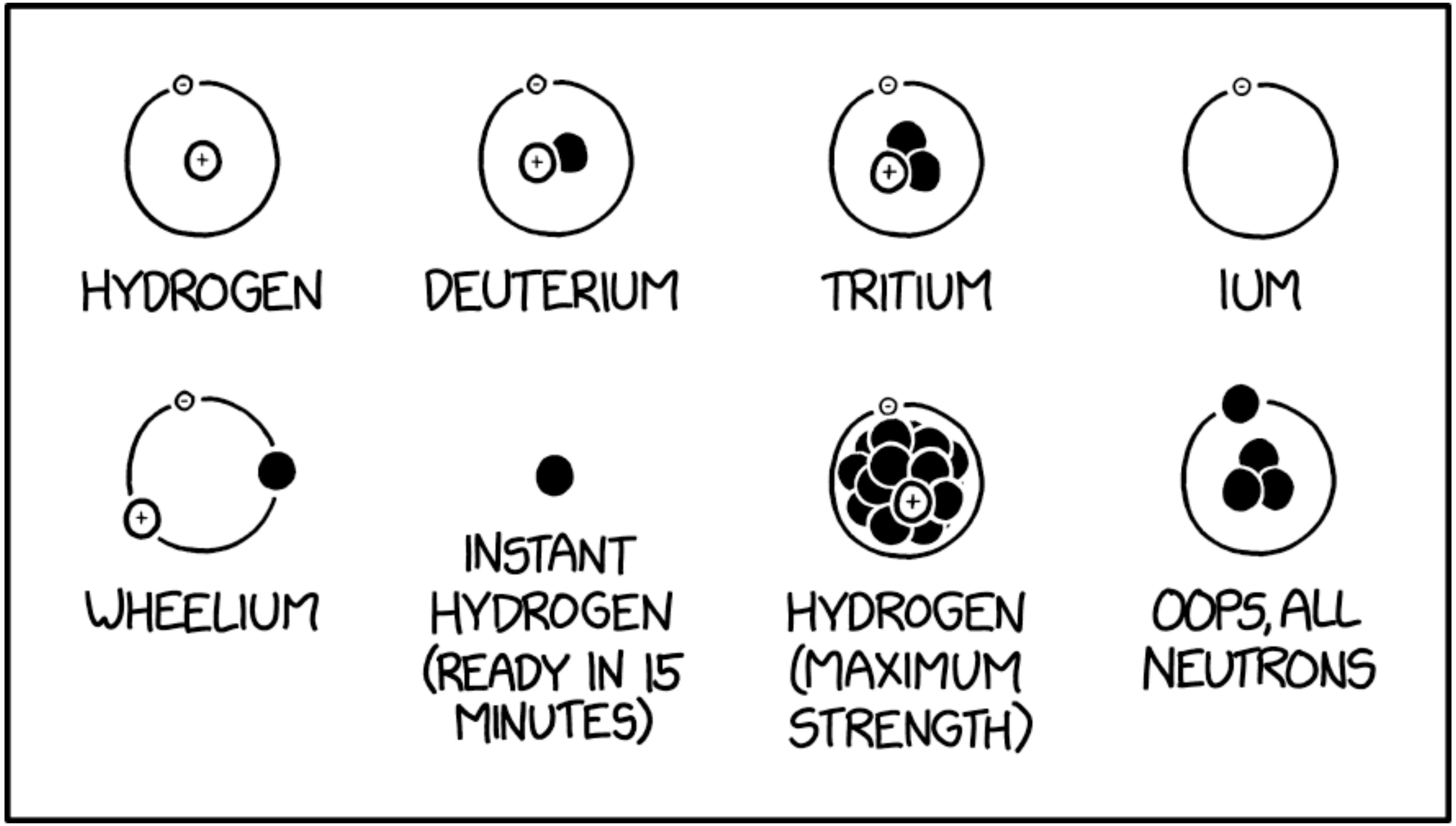

https://xkcd.com/2719/

Plutonium - XKCD

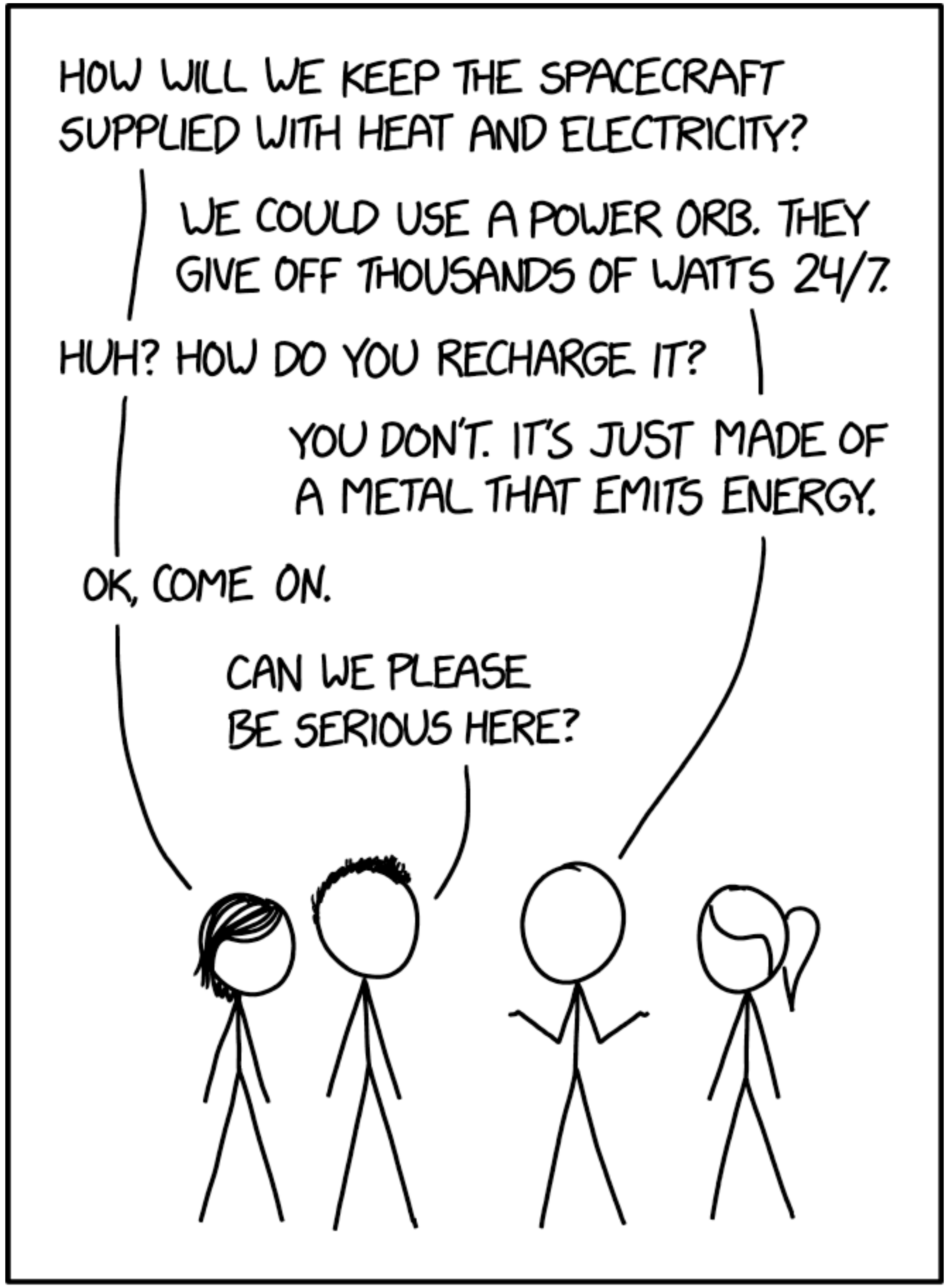

FOR SOMETHING THAT'S REAL, PLUTONIUM IS SO UNREALISTIC.

https://xkcd.com/2115/

Internal conversion

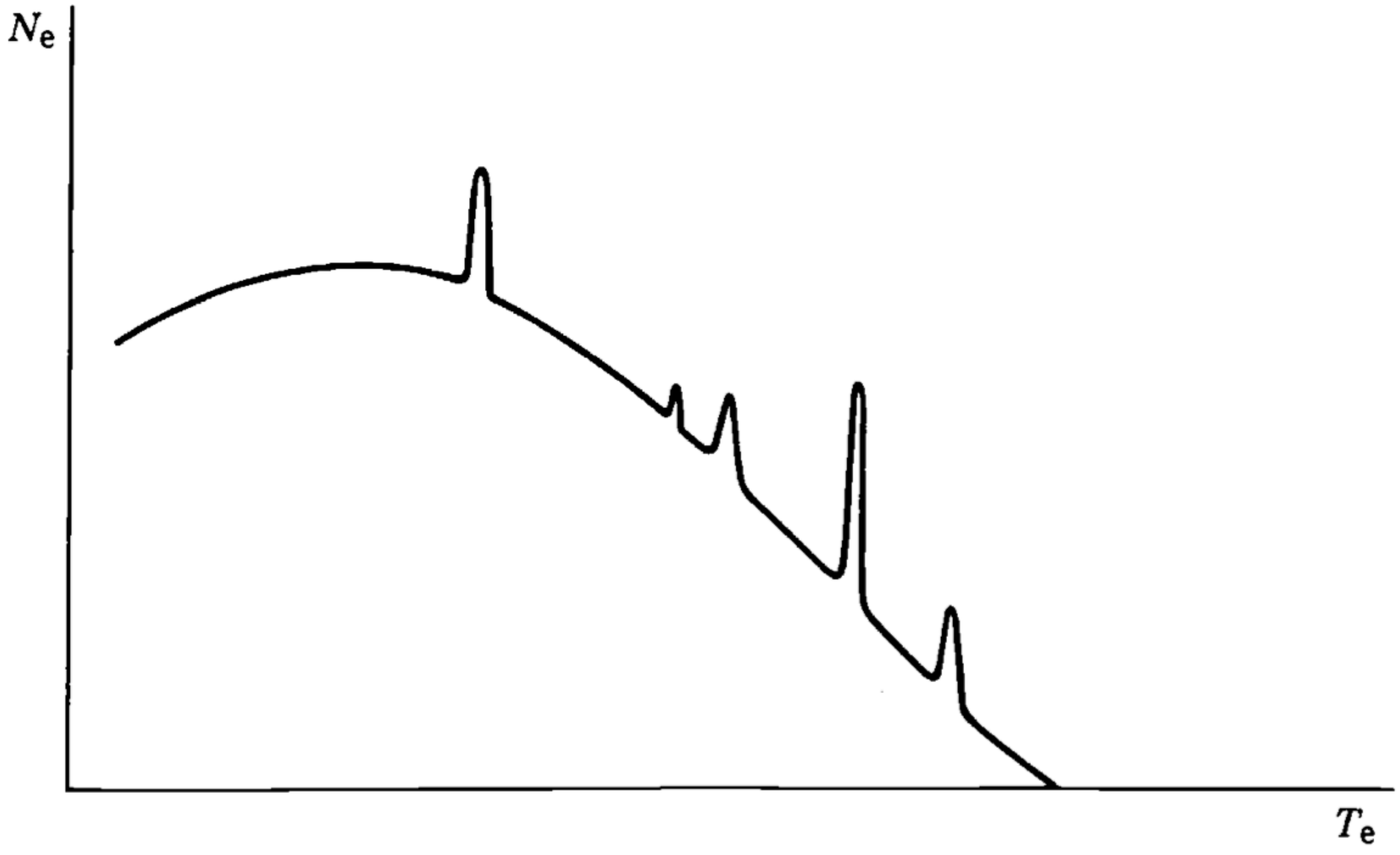

Figure 10.7 A typical electron spectrum such as might be emitted from a radioactive nucleus. A few discrete conversion electron peaks ride on the continuous background from β decay.

Internal conversion

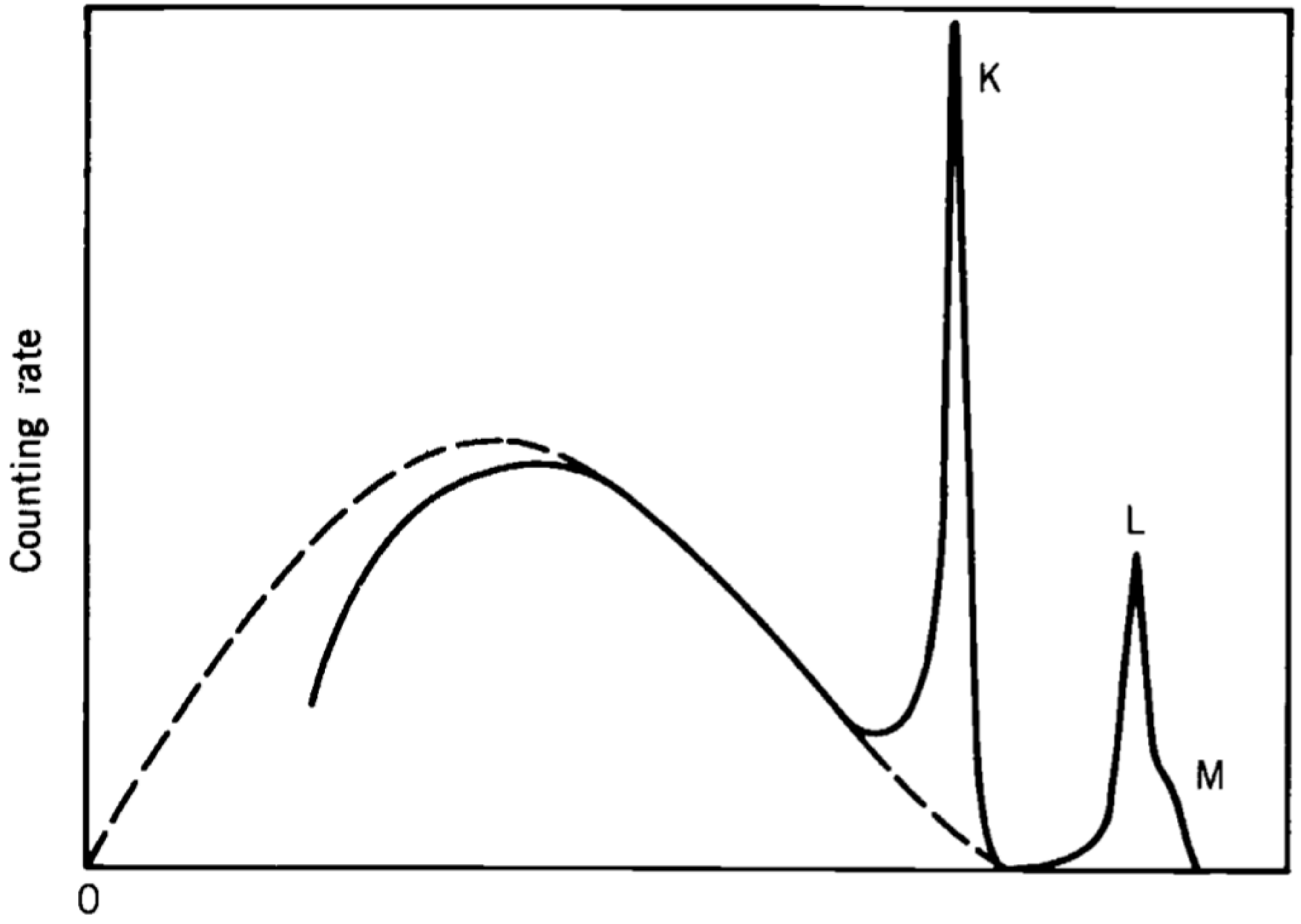

Full spectrum

Higher resolution

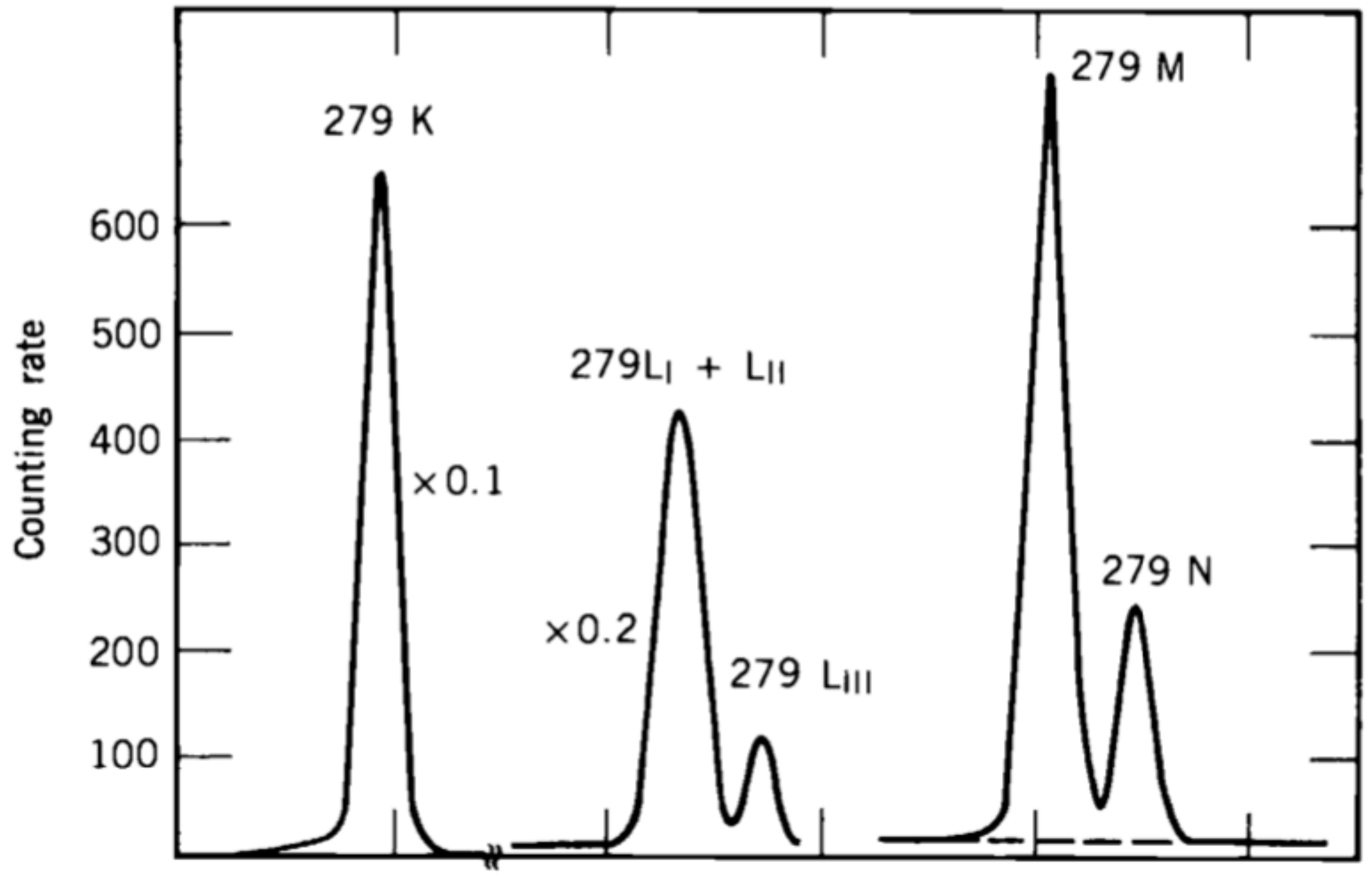

Highest resolution

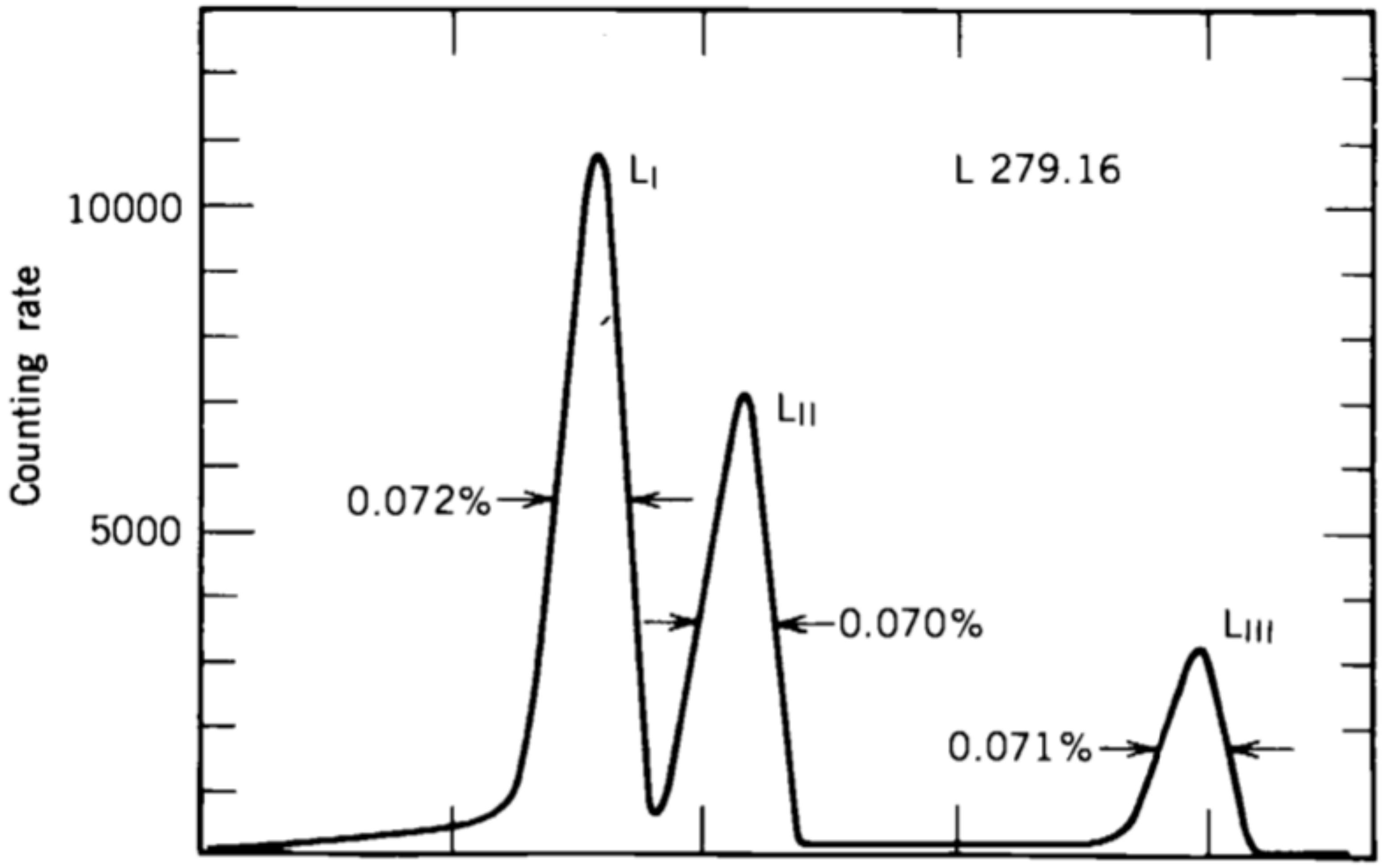

Figure 10.8 Electron spectrum from the decay of ^{203}Hg. At top, the continuous β spectrum can be seen, along with the K and unresolved L and M conversion lines. In the middle is shown the conversion spectrum at higher resolution; the L and M lines are now well separated, and even L_{III} is resolved. At yet higher resolution (bottom) L_I and L_{II} are clearly separated. *Sources*: (top) A. H. Wapstra et al., *Physica* **20**, 169 (1954); (middle) Z. Sujkowski, *Ark. Fys.* **20**, 243 (1961); (bottom) C. J. Herrlander and R. L. Graham, *Nucl. Phys.* **58**, 544 (1964).